32ND INTERNATIONAL COSMIC RAY CONFERENCE, BEIJING 2011


# IceCube's In Ice Radio-Frequency extension

THE ICECUBE COLLABORATION[1], E. CHENG[2], L. RUCKMAN[3], G.S. VARNER[3]
[1]*See special section in these proceedings*
[2]*Dept. of Physics, Univ. of Wisconsin, Madison, WI 53703, USA*
[3] *Dept. of Physics and Astronomy, Univ. of Hawaii, Manoa, HI 96822, USA*

**Abstract:** In preparation for designing a large scale array sensitive to high energy neutrinos (EeV), several Radio Frequency (RF) detectors and calibration equipment were installed with the IceCube neutrino detector at the geographic South Pole between the years 2006–2010. The wide and deep holes drilled for IceCube provided a unique opportunity for deep-ice RF detection studies at depths never surveyed before. The deployed detectors are installed between 5 to 1400 meters deep in the ice, and are sensitive to frequencies in the range of 200 MHz–1 GHz. We will present results of ice properties studies (attenuation length and index of refraction) and environmental noise study.

**Corresponding authors:** Hagar Landsman(*hagar@icecube.wisc.edu*), Mike Richman(*mike.d.richman@gmail.com*), Kara Hoffman(*kara@umd.edu*)
DOI: 10.7529/ICRC2011/V04/1236

**Keywords:** Neutrino, Askaryan, GZK, South Pole, ice properties, attenuation

## 1 Introduction

The concept of high energy neutrino radio frequency detector buried in ice at shallow depths or deployed as a surface array was suggested nearly 30 years ago [1]. The RICE [2] array and the ANITA experiment [3] are already taking advantage of the Askaryan effect and the massive volume of ice in Antarctica for neutrino detection by looking for the coherent radio Cherenkov emission from charge asymmetry in high-energy neutrinos cascades. Future experiments include ARIANNA [4], a surface array on the Ross Ice Shelf, and ARA [5], an in-ice array at shallow depths near the South Pole. Our unique access to IceCube's deep and wide holes have provided us with an opportunity for deploying radio frequency (RF) detectors in the deep Polar ice. These detectors use the communication and time calibration systems developed for IceCube and rely on the experience within the IceCube Collaboration for developing hardware and software and for building and deploying highly-sensitive equipment in the extreme South Pole environment as well as on radio technology expertise from the RICE and ANITA Collaborations. IceCube's deep holes and well-established data handling system provide a unique opportunity for deep-ice RF detection studies.

## 2 Hardware description

### 2.1 Full digitization detectors

IceCube's radio extension modules, consisting of several radio frequency (RF) detectors as well as calibration equipment, were installed on IceCube strings during the austral summers between 2006 and 2010 at depths of $5$ to $1400\,\mathrm{m}$. Each radio module was installed directly above IceCube's digital optical modules (DOMs). The RF components were mechanically attached to the $\sim 3\,\mathrm{km}$-long IceCube main cable (a 5-cm-diameter cable bundle for communication and power) which simply served as a mechanical support; some of the modules, however, were tapped into one of the auxiliary twisted-pairs within the main cable designed for specialized device operations. The main cable, being a massive conducting object, can shadow the RF antennas.

During the first two seasons five detectors capable of full waveform (WF) digitization were deployed. These so called "clusters" consist of four receiving channels equally spaced over $\sim 40\,\mathrm{m}$ along the IceCube cable, a transmitting channel and a central electronics module. Each receiver channel consists of a broadband dipole antenna (with the gain centered at $\sim 400\,\mathrm{MHz}$ in air and $\sim 250\,\mathrm{MHz}$ in ice), and a set of front-end electronics (housed in a metal tube), including filters ($450$ MHz notch filter for rejecting constant interference from the South Pole communica-

tion channel, and 200 MHz high-pass filter) and amplifiers ($\sim 50$ dB low-noise amplifier). An additional $\sim 20$ dB amplification is done at a later stage within the electronic module for a total amplification of $\sim 70$ dB. A schematic of the 2006–2007 cluster is shown in Figure 1. Three clusters were deployed at depth of $\sim 300$ m , and two at $\sim 1400$ m. A detailed description of the electronics installed inside the DRM can be found elsewhere [6, 7].

### 2.2 Transient detectors

The idea of using an array of simple transient sensors to image the unique spatiotemporal signature of neutrino interactions in Antarctic ice was proposed by Gusev and Zheleznykh nearly thirty years ago [1]. In this type of detector system, the pattern of coincident hits among a large number of sensors provides event confirmation, indication of direction and energy, and information for rejecting sporadic noise on the basis of time-of-arrival and amplitude. Six units of transient-prototype-detector were deployed in the 2009–2010 season. Each unit consists of a discone wide-band omni-directional antenna feeding into a Transient Detector Assembly (TDA), an exploratory device, whose block diagram is shown in Figure 1. Each unit is read out using a control motherboard (MB) developed for the IceCube DOM [8]. The IceCube cable and calibration system also facilitates timing calibration and data handling. The units were deployed in pairs above three IceCube strings, with one unit at $z = -5$ m and the other at $z = -35$ m. The Local Coincidence (LC) capabilities of the IceCube MB are also exploited; when LC is enabled, each TDA pair reads out data only if both units in the pair are triggered in some adjustable time window. The rise-time of the output pulse from these units is on the order of 10–20 ns and is largely independent of amplitude.

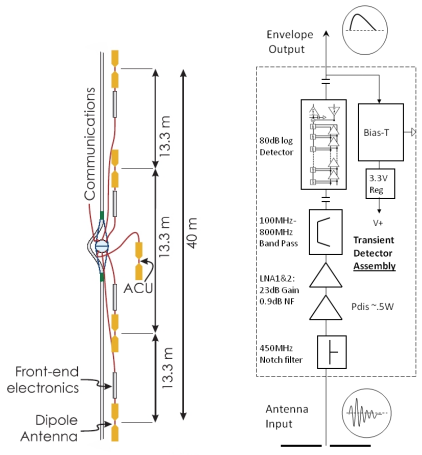


Figure 1: The radio cluster, consisting of the DRM (Digital Radio Module), 4 receiving antennas and 1 transmitting antenna (left); Block diagram of the Transient Detector Assembly (right).

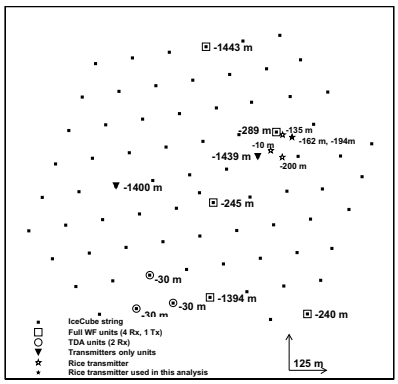


Figure 2: Map of the IceCube radio detector deployments, plotted on top of the full IceCube array. Also shown are the deployment depth of each unit relative to the surface, and the location of the RICE transmitters.

Figure 2 summarizes the in-ice locations and depths of the deployed units.

## 3 Ice Properties

The properties of ice at radio frequencies determine the feasibility and design of future GZK neutrino detectors. Specifically, the attenuation length affects the spacing between channels and the effective detector volume, whereas uncertainties in the index of refraction determine the reconstruction capabilities and simulation quality.

### 3.1 Attenuation Length

The attenuation length $\lambda$ is the distance over which the signal amplitude diminishes by a factor of $e$ due to absorption and/or scattering. In general, $\lambda$ varies with the density and temperature of a medium and with the frequency of the radiation. In South Pole ice, the density and temperature vary with the depth $z$, and so the attenuation length is also a function of depth.

The previous in-ice RF attenuation data from the South Pole were obtained by sending signals down into the ice using a surface transmitter and recording the signals reflected from the bedrock below. This measurement provided an average RF attenuation over the round-trip, weighted by the temperature profile along the path [9].

The IceCube Radio Extension provides us with the first opportunity to make a point-to-point attenuation measurement independent of the unknown bedrock reflection coefficient. Of 20 available receiver channels, we use the 6 which have similar amplifiers and electronics. Our sources are RICE antennas which transmit signals from a pulser operated in an on-site lab. The pulse power can be varied by inserting attenuators in the line. The transmitting antennas are similar to the receiving antennas and are located at var-

ious depths down to 220 m, and up to $\sim 1400$ m away from the receivers (see Figure 2).

The simplest possible relative attenuation measurement would involve broadcasting a signal and measuring the relative power received by antennas at different distances from the transmitter. However, IceCube Radio Extension digitizers have insufficient dynamic range for this approach. Thus, we instead vary the transmitter power, measuring the values which yield the same power at different receivers. The differences between these values are $\Delta\mathcal{L}_{\text{total}}$, the total receiver–receiver difference in losses.

We assume that (in a logarithmic scale) $\Delta\mathcal{L}_{\text{total}} = \Delta\mathcal{L}_{\text{dipole}}(\theta) + \Delta\mathcal{L}_{\text{free space}}(\vec{r}, n(z)) + \Delta\mathcal{L}_{\text{attenuation}}(\vec{r}, \lambda)$. We use a standard dipole pattern for transmitters and receivers: $I(\theta) = (3/8\pi) I_0 \sin^2(\theta)$. The free space losses, which for uniform index of refraction would give the inverse square law, are calculated using ray tracing simulation. After obtaining $\Delta\mathcal{L}_{\text{total}}$ from measurement and $\Delta\mathcal{L}_{\text{dipole}}$ and $\Delta\mathcal{L}_{\text{free space}}$ from simulation, we can calculate the path-averaged attenuation length $\langle\lambda\rangle$: $\Delta\mathcal{L}_{\text{attenuation}} = 10\log_{10} e^{-2\Delta r/\langle\lambda\rangle}$. Figure 3 shows the measurement of pulses from a RICE transmitter. Deep receiver channels show a linear response. Shallow receiver channels have a flatter response for higher power due to saturation; however, for sufficient transmitter attenuation, they also have a linear response.

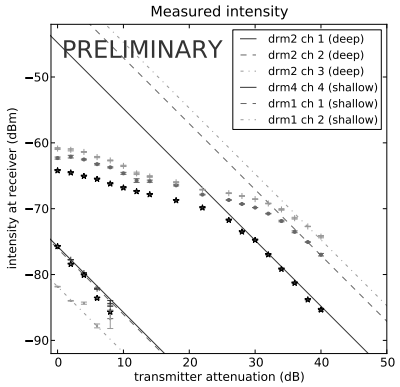


Figure 3: Measured intensity vs. transmitter attenuation.

A linear fit with a slope of $-1$ is done for the linear region on each curve. The difference between the $x$-intercepts for any pair of fits is equal to $\Delta\mathcal{L}_{\text{total}}$ for that antenna pair. To date, sufficient data has been taken only with one of RICE transmitters. Preliminary values obtained from this data for $\langle\lambda\rangle$ range from 400 to 700 meters. These numbers are somewhat lower than past results [9]; however, preliminary systematic error estimates suggest that these results will not be inconsistent with each other.

This measurement is ongoing. Our simulation of the effects of reflection and shadowing by an IceCube cable in the vicinity of a broadband dipole antenna is not yet complete. Other remaining work includes estimating other systematics such as receiver gain uncertainties; taking data with additional transmitters; and combining results for $\langle\lambda\rangle$ with existing density and temperature measurements to obtain a model for $\lambda(z)$.

### 3.2 Index of refraction

Uncertainties in index of refraction lead to uncertainties of the order of a few ns in the time difference measured between two receivers a few meters apart (geometry-dependent); therefore, a precise knowledge of index of refraction is necessary for a sub-ns-resolution detector. The latest index of refraction measurement at the South Pole reported in [10] combines results using the RICE array down to 150 m and ice cores down to 240 m. The model used is of the form $n(z) = n_{\text{deep}} + (n_{\text{shallow}} - n_{\text{deep}})e^{n_c \cdot z}$, where $n_c \approx -0.0132\,\text{m}^{-1}$, $n_{\text{deep}} \approx 1.78$, and $n_{\text{shallow}} \approx 1.35$. The changing index of refraction causes rays to curve in the ice layers, especially in the soft ice layers on top of the glacier (firn), and decreases the angular acceptance of shallow-deployed detectors by causing total reflection of rays propagating between the layers. When looking at possible paths connecting a transmitter and a receiver both in ice there will be either zero or two solutions (direct ray and reflected ray) to the ray-tracing problem. The reflection takes place at the ice-air boundary on the surface, as illustrated in Fig. 4A.

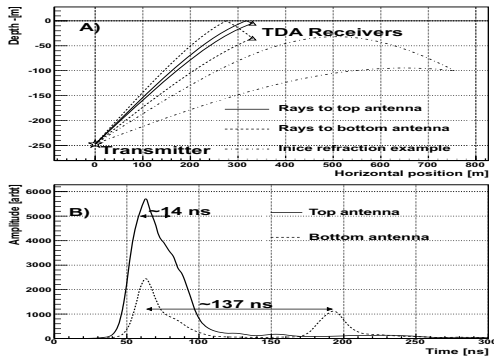


Figure 4: A. Ray Tracing showing the direct- and reflacted-rays solutions. The depths and separation between the transmitter and the receivers in this figure correspond to the transmitter-recievers used in the analysis. B. Average WF collected on the top (solid) and bottom (dashed) antennas of the transient detectors. The time delay between the direct and the refracted ray detected by the bottom antenna is consistent with simulations (137 ns).

The extremely shallow location of the TDA units makes them sensitive to small variations in the index of refraction model, especially to $n_{\text{shallow}}$ and $n_c$. Five out of six TDA units were able to trigger on a calibration pulse transmitted by a calibration antenna from depth of $-245$ m. The sixth unit that did not see the pulser (Top antenna at hole 8)

was in the shaded area where no solution exists. Limits on the ice model parameters can be set by measuring the trigger time differences between different units as well as the time differences between the direct and reflected ray. This is illustrated in Fig 4B where an average WF from a pulser run for the top and bottom detectors is shown. The expected time delay between the direct and reflected ray for the top antenna was calculated to be about $14\,\mathrm{ns}$, and the direct and reflected peaks are not resolvable. For the bottom antenna the simulated time delay was about $137\,\mathrm{ns}$, in good agreement with the measurement. Figure 5 shows preliminary constraints on $n_{\mathrm{shallow}}$ and $n_c$ based on combined time differences measured between detectors.

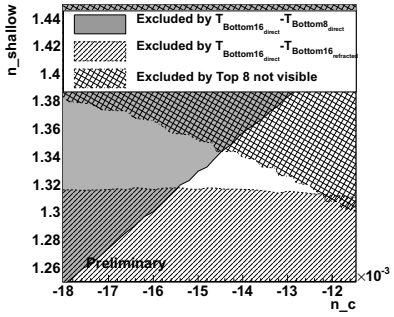


Figure 5: Excluded parameters space for index of refraction based on time delays between hits. This area includes systematic uncertainties from the following uncertainties: timing resolution, slewing, geometry and $n_{\mathrm{deep}}$.

## 4 Environmental Noise

We have previously shown that timing of elevated noise rates coincided with the periods of winds stronger than $\sim 20\,\mathrm{knots}$ (see Figure 6). Since the South Pole is electrically insulated, electrostatic charge accumulates easily, leading to a discharge causing EMI. There are two possible mechanisms as to how electrostatic charge builds up in strong winds: "precipitation charging" [11] where blowing snow causes structures to charge up; and "snowstorm electrification" [12], where charge separation occurs near the snow surface. A preliminary reconstruction study has pointed to an area around large structures in the Dark Sector as the origin of this interference. Preliminary studies with radio detectors away from the station have shown no such interference, supporting the assumption that the noise is originating from structures and not spotaneous charging of the ice. However, additional data are required since this analysis was preformed early in the austral winter, using limited statistics [5].

We were also sensitive to weather balloon launches, happening twice a day. Since this noise source is well defined in time and frequency, it will not be a problem for future detectors.

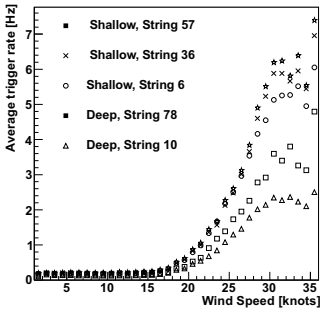


Figure 6: Average trigger rate vs. wind speed for the five clusters described in Section 2.1. The meteorological data were taken from the "Clean Air" automatic weather station, operated by The Antarctic Meteorological Research Center (AMRC) and the Antarctic Automatic Weather Station (AWS) Program [13].

## 5 Summary

IceCube's mature drilling and data acquisition technology have facilitated the deployment of the first fully digital radio test equipment in South Pole ice as well as deployment to greater depths in South Pole ice than was previously possible. Using the IceCube radio frequency extension, we have obtained tighter constraints on the index of refraction model parameters, and an attenuation length measurement is also underway. We have also been able to characterize and understand the RF noise environment at the Pole. This information will provide a valuable guide for the design of a future GZK neutrino detector.

## References

[1] G. A. Gusev, I. M. Zheleznykh, JETP Lett. 38 (1983) 611–614.
[2] I. Kravchenko, et al., Phys. Rev. D73 (2006) 082002.
[3] P. W. Gorham, et al., Phys. Rev. D82 (2010) 022004.
[4] L. Gerhardt, et al., arXiv:1005.5193.
[5] P. Allison, et al., arXiv:1105.2854.
[6] H. Landsman, et al., Nucl. Instrum. Meth. A604 (2009) S70–S75.
[7] H. Landsman, et al., Nucl. Instrum. Meth. In Press, accepted manuscript, (2010) doi:10.1016/j.nima.2010.11.144.
[8] R. Abbasi, et al., Nucl. Instrum. Meth. A601 (2009) 294.
[9] S. Barwick, et al., J. Glaciology 51 (173) (2005) 231.
[10] I. Kravchenko, et al., J. Glaciology 50 (171) (2004) 522.
[11] S. B. Dunham, J. Atmospheric Sciences 23 (1966) 412.
[12] M. Gordon, P. Taylor, Boundary-Layer Meteorology 130 (2009) 97–115.
[13] ftp://amrc.ssec.wisc.edu/pub/southpole/surface_observations.